A chronic hypoxic response in photoreceptors alters the vitreous proteome in mice

Schori, Christian ; Trachsel, Christian ; Grossmann, Jonas ; Barben, Maya ; Klee, Katrin ; Storti, Federica ; Samardzija, Marijana ; Grimm, Christian

Abstract: Reduced oxygenation of the outer retina in the aging eye may activate a chronic hypoxic response in RPE and photoreceptor cells and is considered as a risk factor for the development of age-related macular degeneration (AMD). In mice, a chronically active hypoxic response in the retinal pigment epithelium (RPE) or photoreceptors leads to age-dependent retinal degeneration. To identify proteins that may serve as accessible markers for a chronic hypoxic insult to photoreceptors, we used proteomics to determine the protein composition of the vitreous humor in genetically engineered mice that lack the von Hippel-Lindau tumor suppressor (Vhl) specifically in rods (rod) or cones (all-cone). Absence of VHL leads to constitutively active hypoxia-inducible transcription factors (HIFs) and thus to a molecular response to hypoxia even in normal room air. To discriminate between the consequences of a local response in photoreceptors and systemic hypoxic effects, we also evaluated the vitreous proteome of wild type mice after exposure to acute hypoxia. 1'043 of the identified proteins were common to all three hypoxia models. 257, 258 and 356 proteins were significantly regulated after systemic hypoxia, in rod and in all-cone mice, respectively, at least at one of the analyzed time points. Only few of the regulated proteins were shared by the models indicating that the vitreous proteome is differentially affected by systemic hypoxia and the rod or cone-specific hypoxic response. Similarly, the distinct protein compositions in the individual genetic models at early and late time points suggest regulated, cell-specific and time-dependent processes. Among the proteins commonly regulated in the genetic models, guanylate binding protein 2 (GBP2) showed elevated levels in the vitreous that were accompanied by increased mRNA expression in the retina of both rod and all-cone mice. We hypothesize that some of the differentially regulated proteins at early time points may potentially be used as markers for the detection of a chronic hypoxic response of photoreceptors.

DOI: https://doi.org/10.1016/j.exer.2019.107690

Schori, Christian; Trachsel, Christian; Grossmann, Jonas; Barben, Maya; Klee, Katrin; Storti, Federica; Samardzija, Marijana; Grimm, Christian (2019). A chronic hypoxic response in photoreceptors alters the vitreous proteome in mice. Experimental Eye Research, 185:107690.
DOI: https://doi.org/10.1016/j.exer.2019.107690

Experimental Eye Research 185 (2019) 107690

Contents lists available at ScienceDirect

Experimental Eye Research

journal homepage: www.elsevier.com/locate/yexer

A chronic hypoxic response in photoreceptors alters the vitreous proteome in mice

Christian Schori[a,b], Christian Trachsel[c], Jonas Grossmann[c], Maya Barben[a,d], Katrin Klee[a,b], Federica Storti[a], Marijana Samardzija[a], Christian Grimm[a,b,d,*]

[a] Lab for Retinal Cell Biology, Dept. Ophthalmology, University of Zurich, Zurich, Switzerland
[b] Center for Integrative Human Physiology (ZIHP), University of Zurich, Zurich, Switzerland
[c] Functional Genomics Center Zurich (FGCZ), ETH Zurich and University of Zurich, Zurich, Switzerland
[d] Neuroscience Center Zurich (ZNZ), University of Zurich, Zurich, Switzerland

ARTICLE INFO

Keywords:
Vitreous
Hypoxia
Proteomics
Rod photoreceptors
Cone photoreceptors
Retina

ABSTRACT

Reduced oxygenation of the outer retina in the aging eye may activate a chronic hypoxic response in RPE and photoreceptor cells and is considered as a risk factor for the development of age-related macular degeneration (AMD). In mice, a chronically active hypoxic response in the retinal pigment epithelium (RPE) or photoreceptors leads to age-dependent retinal degeneration. To identify proteins that may serve as accessible markers for a chronic hypoxic insult to photoreceptors, we used proteomics to determine the protein composition of the vitreous humor in genetically engineered mice that lack the von Hippel-Lindau tumor suppressor (*Vhl*) specifically in rods (rod$^{\Delta Vhl}$) or cones (all-cone$^{\Delta Vhl}$). Absence of VHL leads to constitutively active hypoxia-inducible transcription factors (HIFs) and thus to a molecular response to hypoxia even in normal room air. To discriminate between the consequences of a local response in photoreceptors and systemic hypoxic effects, we also evaluated the vitreous proteome of wild type mice after exposure to acute hypoxia.

1′043 of the identified proteins were common to all three hypoxia models. 257, 258 and 356 proteins were significantly regulated after systemic hypoxia, in rod$^{\Delta Vhl}$ and in all-cone$^{\Delta Vhl}$ mice, respectively, at least at one of the analyzed time points. Only few of the regulated proteins were shared by the models indicating that the vitreous proteome is differentially affected by systemic hypoxia and the rod or cone-specific hypoxic response. Similarly, the distinct protein compositions in the individual genetic models at early and late time points suggest regulated, cell-specific and time-dependent processes. Among the proteins commonly regulated in the genetic models, guanylate binding protein 2 (GBP2) showed elevated levels in the vitreous that were accompanied by increased mRNA expression in the retina of both rod$^{\Delta Vhl}$ and all-cone$^{\Delta Vhl}$ mice. We hypothesize that some of the differentially regulated proteins at early time points may potentially be used as markers for the detection of a chronic hypoxic response of photoreceptors.

1. Introduction

More than 20% of people above the age of 75 are affected by age-related macular degeneration (AMD) in Western countries (Wong et al., 2014). The majority (85–90%) of the patients is diagnosed with the non-exudative dry form and only 10–15% suffer from the neovascular wet form of AMD (Ferris et al., 1984; Leibowitz et al., 1980). Whereas wet AMD can be treated with intraocular injections of compounds targeting vascular endothelial growth factor (VEGF) (Brown et al., 2006; Heier et al., 2006; Rosenfeld et al., 2006), a treatment for dry AMD is still an unmet medical need.

It has been suggested that chronically reduced tissue oxygenation (hypoxia) in the ageing eye may be involved in the development of dry AMD (Arjamaa et al., 2009; Feigl, 2009; Stefánsson et al., 2011). While oxygen is supplied to the inner retina by retinal vessels, it is delivered to the outer retina mainly by the choroidal vasculature (Alm and Bill, 1972; Friedman et al., 1964). Thus, proper function of photoreceptors depends on sufficient diffusion or transport of oxygen and nutrients from the vascular choroid to the retina (Linsenmeier and Padnick-Silver, 2000). Age-dependent thinning of the choroid, reduced choroidal blood flow, thickening of Bruch's membrane and accumulation of drusen deposits (Chung et al., 2011; Liu and Xie, 2012) may reduce oxygen availability in the outer retina leading to mild but chronic hypoxia and contribute to the development of retinal disease when a

* Corresponding author. Lab for Retinal Cell Biology, Department of Ophthalmology, University of Zurich, Wagistrasse 14, CH-8952 Schlieren, Switzerland.
E-mail address: cgrimm@opht.uzh.ch (C. Grimm).

https://doi.org/10.1016/j.exer.2019.107690
Received 17 February 2019; Received in revised form 20 May 2019; Accepted 6 June 2019
Available online 07 June 2019

Abbreviations

FDR	false discovery rate
GO	gene ontology
GO-BP	GO-biological process
GO-CC	GO-cellular component
GO-MF	GO-molecular function
GSEA	Gene set enrichment analysis
LC-MS/MS	liquid-chromatography coupled tandem MS
MS	mass-spectrometry
PANTHER	Protein ANalysis THrough Evolutionary Relationships
PRIDE	PRoteomics IDEntifications
VH	vitreous humor
Webgestalt	WEB-based GEne SeT AnaLysis Toolkit

critical threshold is reached (Caprara and Grimm, 2012).

The key factors of the molecular response to reduced tissue oxygenation are the heterodimeric hypoxia-inducible transcription factors (HIF). Under normoxic conditions, HIF-alpha (HIFA) subunits are hydroxylated by prolyl hydroxylases and recognized by the von Hippel-Lindau (VHL) protein complex, which ubiquitinates the hydroxylated HIFAs and targets them to proteasomal degradation. Under hypoxic conditions, HIFA subunits are not hydroxylated and thus not recognized by VHL. They escape proteolytic degradation, translocate to the nucleus, bind to the HIF-beta (HIFB) subunit and regulate the transcriptomic response to hypoxia (Greer et al., 2012). Whereas short-term activation of HIFs may be beneficial and support survival of retinal cells under reduced oxygen conditions (Grimm et al., 2002), chronic activation of HIF2 in the retinal pigment epithelium (RPE) (Kurihara et al., 2016) or HIF1 in photoreceptors (Barben et al., 2018a, 2018b; Lange et al., 2011) leads to retinal degeneration in mice. A therapeutic strategy that reduces HIF levels protects against hypoxia-mediated retinal degeneration (Barben et al., 2018a) and may thus be beneficial for human AMD patients. Such a therapeutic approach depends on the availability of biomarkers that allow the early identification of AMD patients affected by a chronic hypoxic insult in the retina. An early diagnosis would enable a timely intervention increasing the likelihood to successfully preserve vision. Since the retina cannot easily be biopsied in human patients, the vitreous humor (VH), which is assumed to reflect the health state of the retina (Aretz et al., 2013), is investigated as a surrogate tissue.

To work towards the identification of potential biomarkers that might be characteristic for the presence of chronic hypoxia in photoreceptor cells, we analyzed the vitreous proteome of mouse models with an activated molecular response to hypoxia in rods or cones (Barben et al., 2018a, 2018b; Lange et al., 2011). These mice have increased HIFA protein levels, increased expression of HIF target genes and exhibit age-dependent retinal degeneration. Proteomic data from these genetic models were compared to data collected from the vitreous of wild-type mice exposed to systemic hypoxia and to our recently published data from AMD patients (Schori et al., 2018).

2. Material and methods

2.1. Mice

Mice were housed in the animal facility of the University of Zurich and maintained in a 14 : 10 h light-dark cycle with access to food and water *ad libitum*. Animal maintenance and experimentation adhered to the regulations of the veterinary authorities of Kanton Zurich, Switzerland, and the ARVO Statement for the use of animals in ophthalmic and vision research.

Generation and characterization of $Vhl^{flox/flox}$;*OpsinCre* (rod$^{\Delta Vhl}$) and *BPCre;R91W;*$Nrl^{-/-}$;$Vhl^{flox/flox}$ (all-cone$^{\Delta Vhl}$) mice have been described earlier (Barben et al., 2018b; Lange et al., 2011). Rod$^{\Delta Vhl}$ mice have a rod-specific deletion of *Vhl* whereas all-cone$^{\Delta Vhl}$ mice lack *Vhl* in cones of the all-cone retina in *R91W;*$Nrl^{-/-}$ mice (Samardzija et al., 2014). Heterozygous Cre-positive mice were always mated with Cre-negative mice resulting in littermates with or without CRE. Cre-negative mice served as controls. Genotyping was performed by conventional PCR using DNA isolated from ear biopsies and primer pairs as specified elsewhere (Barben et al., 2018b; Lange et al., 2011). All genetic models were on a mixed 129S6/C57BL6 background. *129S6* (Taconic, Ejby, Denmark) wild-type mice were used for the exposure to acute hypoxia (section 2.2).

2.2. Exposure to acute hypoxia

Wild-type mice were placed in a hypoxic chamber and gradually adapted to hypoxic conditions by altering the O_2: N_2 ratio and thereby decreasing the oxygen concentration by 2% every 10 min until a concentration of 7% O_2 was reached. Hypoxic exposure at 7% O_2 lasted for 6 h and VH and retinal tissue were immediately isolated thereafter, as described in section 2.3.

2.3. Vitreous and retina isolation

The VH of mouse eyes was isolated as described by Skeie and coworkers (Skeie et al., 2011) with minor modifications. Briefly, animals were deeply anesthetized with ketamine (130 mg/kg; Parke-Davis; Berlin; Germany)/xylazine (Rompun; 26 mg/kg; Bayer AG; Leverkusen; Germany). After respiration ceased, the heart was exposed and the animal perfused with 10 mL of Dulbecco's phosphate buffered saline (DPBS; Thermo Fisher Scientific; Waltham; MA; U.S.A.) to minimize the risk of blood contamination in the VH during vitrectomy. Lens, VH and retina were removed together through a slit in the cornea and transferred to 50 µL of DPBS. The lens was then carefully separated from the retina thereby releasing the VH into the buffer. This was followed by filtration through 0.1 µm centrifugal filters (Millipore Ultrafree; Merck & Cie; Schaffhausen; Switzerland) for 10 min at 5′000 × *g*. The VH in the flow-through was snap frozen in liquid nitrogen and stored at −80 °C until proteomic measurement. The retinal tissue retained by the filter was stored at −80 °C for transcriptomic analysis.

2.4. Vitreous sample preparation and mass spectrometric measurement

VH samples were subjected to a filter-assisted sample preparation (FASP) digest adapted from Wiśniewski et al. (2009). In brief, VH samples were denatured by 4% sodium dodecyl sulfate (SDS)/0.1 M dithiothreitol, incubated at 95 °C for 5 min and sonicated to disrupt collagen networks. Protein concentrations were determined by a Qubit fluorometric protein assay (Life Technologies; Zug; Switzerland). 20 µg of VH proteins were loaded onto a 30 kDa Nominal Molecular Weight Limit ultrafiltration centrifugal device (Microcon-30 kDa; Merck Millipore), centrifuged, washed with 8 M urea and alkylated with 0.05 M iodoacetamide for 1 min. After washing the membrane with 8 M urea and 0.5 M NaCl, proteins were digested in 120 µL of 0.5 M triethylammonium bicarbonate buffer (pH 8.5) using trypsin (Promega; Dübendorf; Switzerland) at an enzyme to protein ratio of 1:100 (w/w) over night at room temperature. Digested samples were centrifuged and eluted peptides acidified with 0.5% trifluoroacetic acid for the subsequent desalting step by C18 solid phase extraction columns (Sep-Pak Fenisterre; Waters Corp.; Milford; MA; U.S.A.) using 3% acetonitrile/0.1% trifluoroacetic acid. Desalted tryptic peptides were lyophilized and resolubilized in 0.1% formic acid.

Analysis of samples using shotgun proteomics was performed by liquid chromatography coupled to tandem mass spectrometry (LC-MS/

MS) on a high-resolution Orbitrap mass spectrometer (QExactive; Thermo Fisher Scientific; Bremen; Germany). The mass spectrometer was interfaced to a nano-HPLC system (EASY-nLC 1000; Thermo Fisher Scientific) with a self-packed reverse-phase column (75 µm × 10 cm) containing C18 beads (AQ; 3 µm; 200 Å; Bischoff GmbH; Leonberg; Germany) at a flow rate of 200 nL × min^{-1}. The electrospray source was fitted with a 10 µm emitter tip (New Objective; Woburn; MA; USA) with an applied electric potential of 2.2 kV. High accuracy mass spectra were acquired in the mass range of 300–1′700 m/z and a target value of 3×10^6 ions in MS1, followed by higher energy collisional dissociation fragmentation and top-12 MS2 with 30 s of dynamic exclusion. All data are handled and annotated by the local laboratory information management system (LIMS) (Türker et al., 2010).

2.5. Protein identification and quantification

ProgenesisQI for proteomics software (Version 3.0.5995, Nonlinear Dynamics Ltd., Tyne, UK) was used for MS1 intensity-based label-free relative quantification and performed separately for VH samples from acute hypoxic, $rod^{\Delta Vhl}$ and $all\text{-}cone^{\Delta Vhl}$ mice. The peptide ion maps of all samples were aligned to the measurement of a representative pool of 3 samples per genotype and time point. Peptides with a charge state of 2 + to 5 + were retained for quantification. Top five rank tandem mass spectra were exported for each peptide ion using charge deconvolution and deisotoping option at a maximum number of 200 peaks per MS2. The exported mgf file was searched with Mascot database (Version 2.5.1, Matrix Science Ltd., London, UK) with the following search settings: maximum missed cleavages: 2; peptide mass tolerance: 10 ppm; number of $^{13}C = 1$; and fragment ion tolerance: 0.04 Da. Carbamidomethyl formation was specified as fixed modification, whereas oxidation of methionine and acetylation at protein N-terminus were specified as variable modifications and searched against the mouse protein database (Taxonomy ID: 10090) from UniProt (59′783 entries; downloaded: 02.09.2016) concatenated to a decoy (reversed) database and 260 known mass spectrometry contaminants (see appendix B). A target-decoy approach was used to estimate the false-discovery levels (Käll et al., 2008). Decoy hits and proteins with single hit peptides were excluded from further analysis. Relative quantification was performed based on non-conflicting peptides relatively to respective age-matched control groups. Fold change (FC) was calculated and statistical significance determined by one-way ANOVA on the hyperbolic arcsine transformed normalized protein abundance. Significant differential regulation was defined as $|\log_2(FC)| > 0.58$ (FC < 0.67 or FC > 1.5) with a P value < 0.05.

2.6. Data visualization

Categorization of the identified proteins according to their involvement in different gene ontology (GO) processes was performed by PANTHER GO classification database (Version 12.0; Protein ANalysis THrough Evolutionary Relationships; www.pantherdb.org) (Mi et al., 2017). Significantly differentially regulated proteins of each group of mice were categorized in the respective parental GO terms 'biological process' (GO-BP), 'molecular function' (GO-MF) and 'cellular component' (GO-CC).

R (Version 3.4.1) with the 'RcolorBrewer' (Version 1.1–2 by Erich Neuwirth) package was used for the generation of bar charts and volcano plots. Log_2-transformed normalized relative abundances were centered by subtraction of the average relative abundance of each protein. Hierarchical clustering of Pearson correlation for proteins was applied and visualized by heatmap using the R package 'pheatmap' (Version 1.0.8 by Raivo Kolde). The area-proportional VennDiagram was generated by BioVenn (Hulsen et al., 2008). Gene set enrichment analysis (GSEA) was performed with gene lists ranked by $\log_2(FC)$ (Subramanian et al., 2005) using Webgestalt (Version 2017; WEB-based GEne SeT AnaLysis Toolkit; www.webgestalt.org) (Wang et al., 2017) together with data mapping to wikipathways.org (Kutmon et al., 2016). Significance threshold for pathway enrichment was set to a false discovery rate (FDR) < 0.25. The number of samples (n) used for individual experiments is given in the respective results section.

Table 1
Primers used for qPCR.

Gene	Fwd 5′-3′	Rev 5′-3′
Actb	CAACGGCTCCGGCATGTGC	CTCTTGCTCTGGGCCTCG
Adm	TCCTGGTTTCTCGGCTTCTC	ATTCTGTGGCGATGCTCTGA
A2m	TAAATGACGAGGCTGTGCTG	CATCGAGATGAGGATGGAGAA
Cdhr1	CATCCAGGAGCCTTACATCA	CTTGGAGGAGTGTAGGTTCT
Gbp1	GAGAAGATGGAGCAGGAACG	TATGGTGCATGATCGAGGTG
Gbp2	TGATGATGCAGCAGAAGGAA	GCACTTCCCAGACGATTTGT
Hnrnpr	GCATTCATCACCTTCTGTGGA	GGCGAATCTCATAGCTGTCA
Hyi	GTGCTGTATGCCAAGGCT	CATGCTTCAGATTCTCCACAA
Mvp	CAGTCATCAAACAGAACCAAGC	CCACCAGATCCAGCACCTC
Pltp	TCTGGATCTGGTGAAGCAGGA	TGCGTTGGAGATGTTCAGCAG
Serpina3n	GTCTTCTCCACACAGGCTGAC	CAGTTTCGCAGACATTGGGACA
Snap25	TGATGAGTCCCTGGAAAGCAC	ATTTGGTCCATCCCTTCCTCA
Vps35	CTCTCAGGACCAGGTAGATT	GGATCATCAGAACGTAGCAG
Ykt6	ACAAAGGCGATCCGAAAGCG	CCGAGCGTTCCACAATCAGT

2.7. RNA isolation and semi-quantitative real-time PCR

Total RNA was isolated from retinal tissue collected during VH isolation (see 2.3) using an RNA isolation kit (Nucleo Spin RNA, Macherey Nagel, Oensingen, Switzerland) according to manufacturer's instructions with an additional on-column DNaseI treatment. One microgram of RNA was used for reverse transcription with oligo(dT) and MMLV reverse transcriptase (Promega, Dübendorf, Switzerland). Semi-quantitative real-time PCR (qPCR) was performed on a QuantStudio 3 real-time PCR system (Thermo Fisher Scientific) using 10 ng cDNA template with PowerUp SYBR Master Mix (Thermo Fisher Scientific) and appropriate primer pairs (Table 1), which were designed to span large intronic regions and avoid known single nucleotide polymorphisms. Reactions were normalized to β-Actin (*Actb*) and relative expression was calculated by the comparative threshold cycle method ($\Delta\Delta C_T$). Statistical analysis of real-time PCR data was performed by comparing gene expression in experimental mice to their respective controls for each time point individually using a two-tailed t-test. All data are presented as mean values ± standard deviation (SD). The number of samples (n) used for individual experiments is given in the respective results section.

3. Results

VH samples isolated from i) wild-type mice exposed to acute hypoxia for 6 h; ii) 10-, 16- and 30-week-old $rod^{\Delta Vhl}$ mice and iii) 4-, 8- and 12-week-old $all\text{-}cone^{\Delta Vhl}$ mice were subjected to LC-MS/MS analysis. The time points of analysis of the genetic models reflect states prior to gross morphological changes in the retina, ongoing early degeneration, and late degeneration (Barben et al., 2018a, 2018b). Relative label-free quantification was performed by comparison of the experimental groups with their respective age-matched controls for each time point. The mass spectrometry proteomics data were handled using the local LIMS (Türker et al., 2010) and all relevant data have been deposited to the ProteomeXchange Consortium via the PRIDE (Vizcaíno et al., 2016) partner repository with the data set identifier PXD008911.

3.1. Changes in the vitreous proteome after acute hypoxia

1′357 unique proteins with an estimated FDR of 2% were identified in the VH of normoxic mice and mice exposed to acute hypoxia (Table A.1; N = 3). Of these, 257 proteins were significantly (P < 0.05)

regulated with a $|\log_2(FC)| > 0.58$, resulting in 159 up- and 98 down-regulated proteins (Fig. 1A, Table A.1). Principal component analysis (data not shown) and hierarchical clustering of Pearson correlation analysis discriminated the VH samples of hypoxic mice from their respective normoxic controls (Fig. 1B). GSEA identified TCA cycle and PluriNetWork (Som et al., 2010) as the most strongly regulated pathways upon acute hypoxia (Table 2). Several proteins with reported hypoxia-regulated expression such as leucine-rich repeat-containing protein 47 (LRC47) (Ma et al., 2015), synapsin-1 (SYN1) (Hu et al., 2014) and fatty acid-binding protein 7 (FABP7 (alias E9Q0H6)) (Bensaad et al., 2014; Qiang et al., 2012) were identified among the top 10 up-regulated proteins (Table 3). In addition, ribonuclear protein HNRNPL (alias G5E924) is also connected to hypoxia as it translocates to the cytoplasm where it may associate with VEGF mRNA in reduced oxygen conditions (Shih and Claffey, 1999). Interestingly, 8 of the top 10 down-regulated proteins were crystallins and in general all 16 significantly regulated crystallins were reduced in the VH of hypoxic mice (Table 3 and A.1).

3.2. Changes in the vitreous proteome of rod$^{\Delta Vhl}$ mice, a model for a chronic hypoxic response in rods

As reported earlier, the retina of rod$^{\Delta Vhl}$ mice degenerates slowly but progressively starting at around 10 weeks of age (Barben et al., 2018a; Lange et al., 2011). Proteomic analysis at an early (10 weeks, initial signs of degeneration visible), intermediate (16 weeks, ongoing degeneration) and late (30 weeks, degeneration almost complete) time point identified 1′624 unique proteins with an estimated FDR of 0.8% on protein level (Table A.2, N = 5 for each group). Of these, 60 proteins (41 up- and 19 down-regulated at 10 weeks), 120 proteins (92 up- and 28 down-regulated at 16 weeks) and 78 proteins (51 up- and 27 down-regulated at 30 weeks), respectively, were significantly regulated at the 3 time points with a $|\log_2(FC)| > 0.58$ and $P < 0.05$ (Fig. 2A, Table A.2). Apart from 2 samples of the 10-week-old mice, a time point when the degenerative process is still weak, Pearson hierarchical clustering correctly separated the rod$^{\Delta Vhl}$ mice from the respective control mice (Fig. 2B).

Among the significantly regulated proteins, only interferon-induced GBP2 was found up-regulated at all three time points (Fig. 2C, Table A.2). Although levels of synaptobrevin homolog YKT6 (YKT6) were also significantly changed at all three time points, this protein was inconsistently regulated showing an increase at 16 weeks of age (2.4-fold) and a reduction at 10 and at 30 weeks (1.7-fold and 1.8-fold, respectively) (Fig. 2C, Table A.2).

Despite the identification of proteins encoded by hypoxia-regulated genes such as major vault protein (MVP) (Lara et al., 2009), guanylate-binding protein 1 (GBP1) (Hwang et al., 2006) and vasorin (VASN) (Choksi et al., 2011; Man et al., 2018) among the top up-regulated proteins (Table 4), GSEA analysis did not identify 'hypoxic pathway' as being significantly regulated in the VH of rod$^{\Delta Vhl}$ mice. Instead, 'Complement and Coagulation Cascades' and 'Blood Clotting Cascade' were identified as significantly regulated pathways (FDR < 0.25) in 10-week-old mice (Table 2). No pathway was found enriched in 16- and 30-week-old mice. Interestingly, the complement and coagulation cascade was also found enriched in all-cone$^{\Delta Vhl}$ mice at the early time point (see below).

3.3. Changes in the vitreous proteome of all-cone$^{\Delta Vhl}$ mice, a model for a chronic hypoxic response in cones

The presumed reduced oxygen supply through changes in the choroidal vasculature of the ageing eye would not only affect rods but also cones. To overcome the low abundance of cones in the normal mouse retina, which makes it difficult to investigate cone-specific events, we analyzed the protein composition of the VH in the all-cone retina of *R91W;Nrl*$^{-/-}$ mice (Samardzija et al., 2014). Similar to rods in rod$^{\Delta Vhl}$ mice, a chronic hypoxic state of cones was modeled in *R91W;Nrl*$^{-/-}$ mice by the deletion of *Vhl* from cones (all-cone$^{\Delta Vhl}$) (Barben et al., 2018b). Compared to rod$^{\Delta Vhl}$ mice, the hypoxic response is activated earlier in these mice and initial weak signs of cone degeneration are already visible at 4 weeks of age. At 8 weeks of age, degeneration is strongly ongoing and at 12 weeks many cones are already lost (Barben et al., 2018b).

The collective analysis of the VH proteomes of all-cone$^{\Delta Vhl}$ mice and their respective controls (4 and 8 weeks, N = 6; 12 weeks, N = 5) identified 1′895 unique proteins (Table A.3) with an estimated FDR of 1.8% on protein level. Only 10 proteins were significantly regulated at the early time point (4 weeks of age) with a $|\log_2(FC)| > 0.58$ and $P < 0.05$. Seven of these proteins were up- and 3 were down-regulated (Table 5). At the intermediate time point (8 weeks), 58 of 97 significantly regulated proteins were up-regulated. Finally, 235 out of 294 regulated proteins were increased at the late time point (12 weeks) (Fig. 3A, Table A.3). Heatmap representation of hierarchical cluster analysis of Pearson correlation for individual proteins and mice showed good clustering of the VH samples for the same genotype at all three time points (Fig. 3B).

None of the differentially regulated proteins in 4-week-old mice overlapped with the 8-week group (Fig. 3C, Table A.3). Corticosteroid-binding globulin (CBG), also known as transcortin encoded by *Serpina6*, was the only overlapping protein between the 4- and 12-week groups (2.1- and 4.0-fold up-regulated, respectively; Fig. 3C, Table A.3). A tendency to increased CBG levels was also found at 8 weeks (2.7-fold)

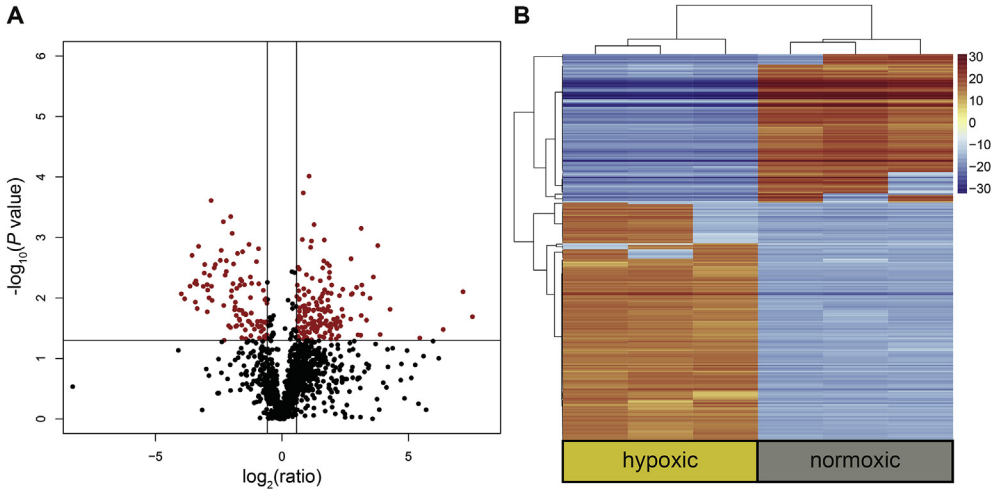

Fig. 1. Changes of the vitreous proteome after exposure of wild type mice to acute hypoxia. A) Volcano plot of all identified proteins. Significantly differentially regulated proteins ($|\log_2(FC)| > 0.58$, x-axis; $P < 0.05$ ($-\log_{10}$), y-axis) are shown in red. **B)** Heat map representation with hierarchical clustering of Pearson correlations for individual proteins (rows) and mice (columns) of all significantly differentially regulated proteins. Shades of red: up-regulated proteins; shades of blue: down-regulated proteins. N = 3.

Table 2
Significant GSEA enriched pathways (log_2(FC) ranking) in mice exposed to acute hypoxia and in rod$^{\Delta Vhl}$ and all-cone$^{\Delta Vhl}$ mice at the early time point.

ID	Enriched Pathway	FDR*	NES**	Enriched Genes
Acute hypoxia				
WP434	TCA Cycle	0.065	1.70	*Aco2, Cs, Dld, Mdh2, Dlat, Idh3a*
WP1763	PluriNetWork	0.110	1.72	*H3f3a, Hcfc1, Kpna2, Mef2d, Prkaca, Sf1, Mta2, Pin1, Usp7, Gsk3b, Wdr61*
rod$^{\Delta Vhl}$, 10w				
WP449	Complement and Coagulation Cascades	0.022	1.79	*Fgb, Cfd, C1qb, C4b, Cfh, Cfi, F2, Plg, Serpinf2, A2m*
WP460	Blood Clotting Cascade	0.231	1.63	*Fgb, F2, Fga, Plg, Serpinf2, Fgg*
all-cone$^{\Delta Vhl}$, 4w				
WP216	Striated Muscle Contraction	0.198	1.90	*Tpm2, Ttn, Tpm4*
WP449	Complement Coagulation Cascades	0.239	1.94	*Cfd, Serpinc1, Serping1, C3, C4b, Cfi, Kng1, Plg, Serpinf2, F12*

* *FDR < 0.25 is considered significant;* ** *Normalized enrichment score.*

Table 3
Top 10 up- and down-regulated proteins after exposure to acute hypoxia.

Acute hypoxia									
up-regulated					down-regulated				
protein name	gene name	unique peptides	log_2(FC)	*P* value	protein name	gene name	unique peptides	log_2(FC)	*P* value
LRC47	*Lrrc47*	2	> 10.0	< 0.0000	CRYAA	*Cryaa*	2	−4.0	0.0085
SYN1	*Syn1*	2	7.5	0.0204	CRYAB	*Cryab*	29	−3.8	0.0103
Q91V77	*S100a1*	6	7.2	0.0079	CRBB1	*Crybb1*	29	−3.6	0.0064
Q8BVQ0	*Wdr61*	2	6.4	0.0333	CRGE	*Cryge*	12	−3.6	0.0020
PNPO	*Pnpo*	2	5.4	0.0459	Q9QXC6	*Cryba1*	37	−3.4	0.0057
E9Q0H6	*Fabp7*	2	4.3	0.0154	VPS35	*Vps35*	9	−3.4	0.0117
DCNL1	*Dcun1d1*	1	3.9	0.0402	CRBB3	*Crybb3*	17	−3.4	0.0052
D3Z061	*Uba6*	3	3.8	0.0014	CRBA4	*Cryba4*	14	−3.4	0.0059
SPS2	*Sephs2*	3	3.6	0.0045	LGSN	*Lgsn*	26	−3.3	0.0149
G5E924	*Hnrnpl*	1	3.5	0.0101	CRGD	*Crygd*	11	−3.3	0.0014

but with a high p-value (0.6414). In contrast to the comparisons involving the 4-week time point, 44 proteins were found significantly and commonly regulated at the 8- and 12-week time points (Fig. 3C, Table A.3).

GSEA of 4-week-old all-cone$^{\Delta Vhl}$ mice identified 'striated muscle contraction' and - similar to rod$^{\Delta Vhl}$ mice - 'complement and coagulation cascades' to be differentially regulated (Table 2). Among the genes found enriched within the 'complement and coagulation cascade' complement factor D (*Cfd)*, complement C4–B (*C4b)* and complement factor I (*Cfi)* were upregulated in both rod$^{\Delta Vhl}$ (4-, 2.6- and 15.4-fold, respectively) and all-cone$^{\Delta Vhl}$ mice (1.8-, 1.7- and 2.2-fold, respectively) (Tables A.2 and A.3). No pathway was significantly enriched in 8-week-old mice. In 12-week-old all-cone$^{\Delta Vhl}$ mice, we found 'mRNA processing' (FDR: 0.165), 'IL-5 signaling pathway' (FDR: 0.197), 'blood clotting cascade' (FDR: 0.200) and 'type II interferon signaling (IFGN)' (FDR: 0.241) to be enriched (not shown).

3.4. Gene ontology term analysis

GO term analysis of all significantly regulated proteins in rod$^{\Delta Vhl}$ and all-cone$^{\Delta Vhl}$ mice revealed that several GO-MF terms changed similarly over time in both types of mice. 'Binding' and 'structural molecule activity' increased whereas 'receptor activity', 'signal transducer activity' and 'transporter activity' decreased with age (Fig. 4). For GO-BP and GO-CC, data from rod$^{\Delta Vhl}$ rather differed from those of all-cone$^{\Delta Vhl}$ mice. Whereas the GO-BP term 'localization' and GO-CC term 'cell part' declined in rod$^{\Delta Vhl}$, they rather increased in cone$^{\Delta Vhl}$ mice. In contrast, the GO-BP term 'multicellular organismal process' and the GO-CC term 'macromolecular complex' increased in rod$^{\Delta Vhl}$ but decreased in cone$^{\Delta Vhl}$ mice. Only the GO-BP term 'biological regulation' had the same increasing tendency in both mice (Fig. 4).

3.5. Correlation of the VH proteome with gene expression in the retina

Changes of the vitreous proteome may be directly or indirectly caused by gene expression changes in the retina. To test this, we analyzed retinal mRNA levels of individual genes by real-time PCR and compared FC of retinal mRNA to FC of the respective proteins in the VH (Fig. 5). As a control, we verified increased expression of adrenomedullin (*Adm*) mRNA, a known hypoxia-regulated gene (Sena et al., 2014). Whereas *Adm* was only mildly up-regulated in acute hypoxia (Fig. 5A), we detected strongly increased *Adm* mRNA levels in both rod$^{\Delta Vhl}$ and all-cone$^{\Delta Vhl}$ mice (Fig. 5B and C). In both groups, *Adm* levels dropped at the last time point, presumably due to degeneration of the cells with a chronically activated hypoxic response (Barben et al., 2018a, 2018b; Lange et al., 2011).

Genes to be tested by qPCR were selected based on significant regulation of the respective proteins in more than one mouse group. Moreover, genes such as vacuolar protein sorting-associated protein 35 (*Vps35*), *Mvp* and cadherin-related family member 1 (*Cdhr1)* that were specific for the hypoxic, the rod$^{\Delta Vhl}$, or the all-cone$^{\Delta Vhl}$ group, respectively, were also included. In general, correlation between retinal gene expression and VH protein levels was poor for the acute hypoxia group (Fig. 5A) and better for the genetic models (Fig. 5B and C).

In rod$^{\Delta Vhl}$ mice, increased VH protein levels were mirrored by increased retinal expression for alpha-2 macroglobulin (*A2m)*, *Gbp1, Gbp2* and *Mvp* (Fig. 5B). Decreased levels were reflected by a tendency of reduced expression of hydroxypyruvate isomerase (putative; *Hyi*). No

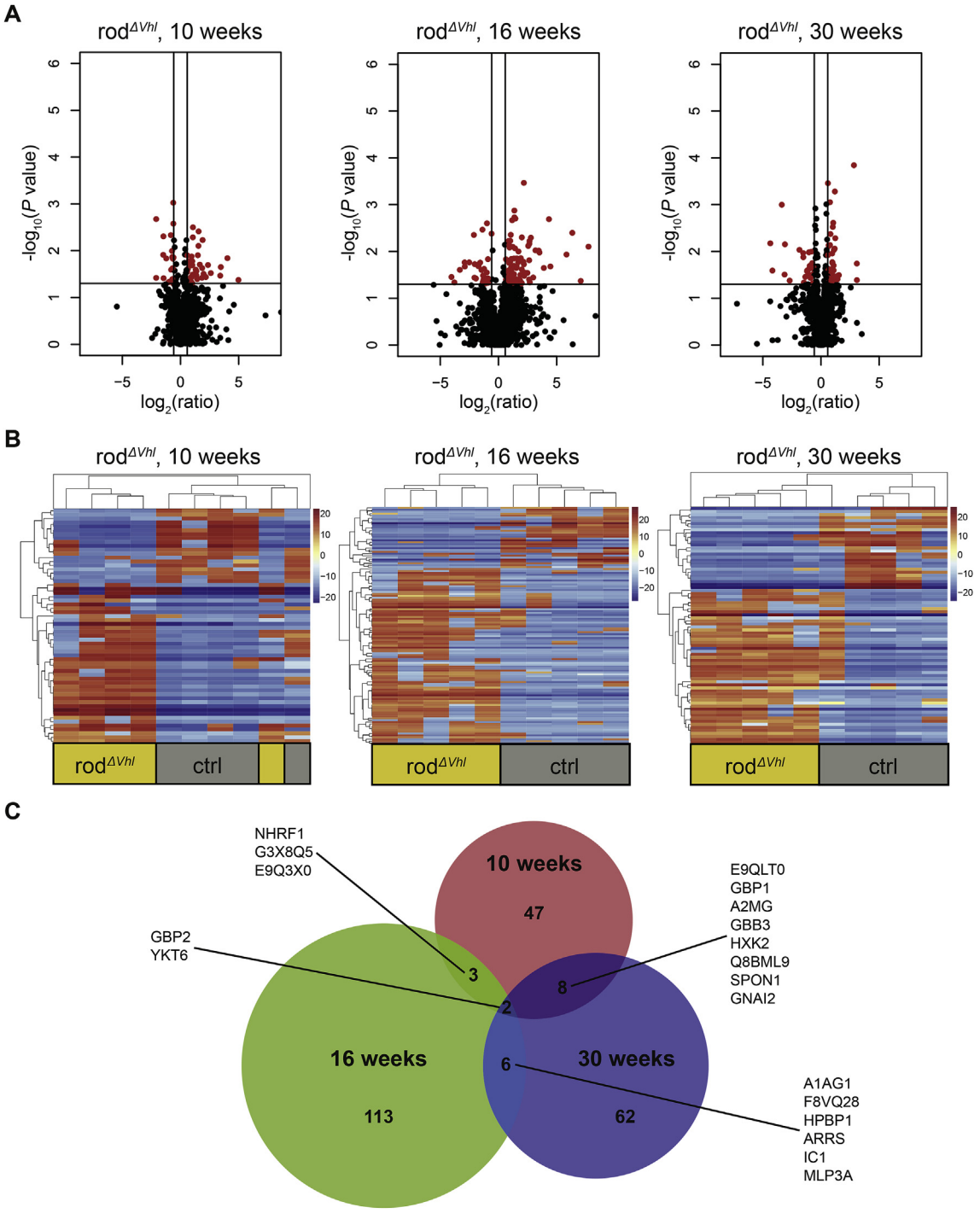

Fig. 2. Changes of the vitreous proteome in rod$^{\Delta Vhl}$ mice during ageing. A) Volcano plot of all identified proteins. Significantly differentially regulated proteins ($|\log_2(FC)| > 0.58$, x-axis; $P < 0.05$ ($-\log_{10}$), y-axis) are shown in red. **B)** Heat map representation with hierarchical clustering of Pearson correlation of all significantly differentially regulated proteins (rows) in individual mice (columns). Shades of red: up-regulated proteins; shades of blue: down-regulated proteins by *Vhl* knockdown in rods. Columns marked with yellow represent rod$^{\Delta Vhl}$ samples, columns marked in grey represent controls. **C)** Venn diagram of significantly differentially regulated proteins ($|\log_2(FC)| > 0.58$; $P < 0.05$) of rod$^{\Delta Vhl}$ mice at indicated time points. N = 5.

clear correlation was established for heterogeneous nuclear ribonucleoprotein R (*Hnrnpr*), phospholipid transfer protein (*Pltp*), serpin family A member 3 (*Serpina3a*), synaptosomal-associated protein 25 (*Snap25)* and *Ykt6* (Fig. 5B).

In all-cone$^{\Delta Vhl}$ mice, increased VH protein levels correlated with increased retinal expression of *Gbp2* and serine protease inhibitor A3N (*Serpina3n)*, and decreased protein levels with reduced gene expression of *Cdhr1* (Fig. 5C). Even though *A2m* and *Hyi* were expressed at increased levels in all-cone$^{\Delta Vhl}$ mice at all time points, VH levels of the respective proteins were reduced. *Hnrnpr* and *Snap25* were decreased at the gene but increased at the protein level (Fig. 5C). No consistent increased or reduced gene expression pattern or protein levels were established for *Gbp1, Pltp* and *Ykt6*.

It is interesting to note that the correlation between protein levels in the VH and gene expression in the retina was different in all-cone$^{\Delta Vhl}$ and rod$^{\Delta Vhl}$ mice, suggesting that lack of *Vhl* in rods or cones affected

Table 4
Top 10 up- and down-regulated proteins in rod$^{\Delta Vhl}$ mice at each time point.

up-regulated					down-regulated				
protein name	gene name	unique peptides	log_2(FC)	*P* value	protein name	gene name	unique peptides	log_2(FC)	*P* value
10-week-old									
VASN	*Vasn*	4	5.0	0.0422	BFSP2	*Bfsp2*	24	−2.1	0.0380
B1AVU4	*Gm14744*	3	4.0	0.0144	PYGL	*Pygl*	15	−2.1	0.0021
E9Q3X0	*Mvp*	3	3.5	0.0223	A2A4A1	*Dnajc24*	1	−1.5	0.0122
Q3ULB1	*Tes*	4	3.4	0.0341	CRK	*Crk*	10	−1.5	0.0049
GBP4	*Gbp4*	1	2.6	0.0301	GNAI2	*Gnai2*	4	−1.5	0.0387
CBG	*Serpina6*	2	2.4	0.0202	E9QLT0	*Hyi*	3	−1.2	0.0146
HPT	*Hp*	5	2.2	0.0365	MYH9	*Myh9*	61	−1.0	0.0468
GBP1	*Gbp1*	8	2.0	0.0313	BZW1	*Bzw1*	3	−0.9	0.0451
A2MG	*A2m*	96	1.9	0.0059	PLAP	*Plaa*	5	−0.8	0.0046
PSB9	*Psmb9*	2	1.9	0.0235	SYT1	*Syt1*	5	−0.8	0.0255
16-week-old									
PIGR	*Pigr*	1	> 10.0	0.0108	RACK1	*Rack1*	13	−4.0	0.0351
F8WHR6	*Ddx46*	2	> 10.0	0.0115	TAGL2	*Tagln2*	8	−3.8	0.0458
NUDT5	*Nudt5*	1	7.7	0.0079	NMT1	*Nmt1*	3	−3.3	0.0247
EPM2A	*Epm2a*	2	6.3	0.0040	A2AWI7	*Sh3glb2*	2	−2.9	0.0172
SNP25	*Snap25*	2	5.8	0.0116	LSM12	*Lsm12*	2	−2.9	0.0211
A0A0A6YYE7	*Igkv4-57*	1	4.5	0.0209	COPA	*Copa*	17	−2.5	0.0171
SEPT4	*Sept4*	1	4.3	0.0020	PUR2	*Gart*	13	−2.1	0.0044
BZW2	*Bzw2*	2	3.5	0.0105	ARF1	*Arf1*	11	−2.1	0.0363
B1AVM1	*Gm12887*	2	3.5	0.0096	DNJA1	*Dnaja1*	7	−2.0	0.0186
H3BK03	*Pon1*	2	3.2	0.0095	G5E8R8	*Ubxn7*	5	−1.9	0.0378
30-week-old									
LIPR1	*Pnliprp1*	3	3.1	0.0410	ARFG3	*Arfgap3*	2	−4.4	0.0067
HPBP1	*Hspbp1*	2	3.1	0.0181	IF44L	*Ifi44l*	2	−4.2	0.0256
GBP1	*Gbp1*	8	2.8	0.0001	A1AG1	*Orm1*	3	−3.4	0.0010
SYCC	*Cars*	2	1.5	0.0321	AKT2	*Akt2*	2	−3.1	0.0312
A2AIM4	*Tpm2*	1	1.4	0.0389	E9QLT0	*Hyi*	3	−3.1	< 0.0001
PTBP2	*Ptbp2*	2	1.4	0.0332	F8VQ28	*Pxn*	1	−3.1	0.0070
A8R0U9	*Esp16*	1	1.2	0.0455	CRBB3	*Crybb3*	29	−2.7	0.0420
REEP6	*Reep6*	4	1.2	0.0052	RTN3	*Rtn3*	6	−1.9	0.0092
A2MG	*A2m*	96	1.2	0.0005	NFASC	*Nfasc*	17	−1.5	0.0108
FBLN1	*Fbln1*	7	1.2	0.0087	GNAI2	*Gnai2*	4	−1.5	0.0133

the respective VH protein composition differently. *Gbp2*, however, was up-regulated on gene and protein levels in both genetic models (Fig. 5B and C).

4. Discussion

Proteins released by the retina may be detected in the VH (Monteiro et al., 2015) and serve as indicators of the integrity and/or health status of the retina. Reports on the vitreous proteome of patients with diabetic retinopathy (Gao et al., 2008; Loukovaara et al., 2015; Shitama et al., 2008; Wang et al., 2013; Yamane et al., 2003), wet AMD (Koss et al., 2014; Nobl et al., 2016) and dry AMD (Schori et al., 2018) have been published. Proteomic data for the VH of mouse models for retinal degenerative diseases, however, are sparse, likely reflecting the difficulty to collect sufficient material for analysis. Nevertheless, proteomic data for the VH have been presented for the wild type mouse (Skeie and Mahajan, 2013), and for models of myopia (Cases et al., 2017) and proliferative vitreoretinopathy (Márkus et al., 2017). Since hypoxia is suggested to be a contributing factor to AMD development (Arjamaa et al., 2009; Feigl, 2009; Stefánsson et al., 2011), it may be relevant to investigate the VH proteome of mice exposed to acute systemic hypoxia and mice with a chronic hypoxic response in photoreceptors (Barben et al., 2018a, 2018b; Lange et al., 2011). Since we aimed at the identification of potential VH markers that might indicate a chronic hypoxic insult to mouse photoreceptors we focused primarily on up-regulated proteins, as an increase of a marker is more reliably detected than a reduction.

The distinct VH proteome of mice after exposure to acute hypoxia (Fig. 1) not only demonstrated the dynamic nature of the VH proteome but also suggested that its composition may reflect the adaptation of the mouse to this specific systemic condition. Thus, the generally poor correlation between VH proteome and retinal gene expression in the acute hypoxia model is not surprising as systemic effects may mask the retina-specific contribution to the VH proteome in this model. The better correlation observed for the genetic models supported this notion since any changes in the VH of these mice may have been directly or indirectly caused by the local activation of HIFs in rods or cones.

The adaptation to acute systemic hypoxia may strongly differ from the cell-type specific molecular response to hypoxia that may be relevant for photoreceptors of the ageing eye. This difference is reflected by the low number of differentially regulated proteins that were common to mice after acute hypoxia and transgenic mice with increased levels of HIF transcription factors in rods or cones. Of the top regulated proteins, only SNP25 showed a similar trend in all models (Fig. 5, Tables A.1, A.2, A.3). The increased presence of the protein in the VH, however, was not reflected by changes on the gene expression level, which either indicates a posttranslational regulation, a differential release from cellular structures or a systemic effect. Since SNP25 localizes to both plexiform layers (Hirano et al., 2011) the increased presence of SNP25 in the mouse VH may indicate changes in the synaptic architecture of the retina under the investigated conditions. The slight upregulation of PDZ and LIM domain protein 5 (PDLI5) in the

Table 5
Top 10 up- and down-regulated proteins in all-cone$^{\Delta Vhl}$ mice at each time point.

up-regulated					down-regulated				
protein name	gene name	unique peptides	log_2(FC)	*P* value	Protein name	gene name	unique peptides	log_2(FC)	*P* value
4-week-old									
A2AIM4	*Tpm2*	2	> 10.0	0.0252	RBM24	*Rbm24*	2	−2.2	0.0351
A2CES4	*Snrpb2*	1	1.7	0.0373	IPYR2	*Ppa2*	11	−0.8	0.0049
CBG	*Serpina6*	2	1.1	0.0471	HMGN5	*Hmgn5*	4	−0.8	0.0102
E9Q7P0	*Dnah17*	1	0.9	0.0395					
CNN3	*Cnn3*	18	0.7	0.0435					
MK09	*Mapk9*	3	0.7	0.0093					
VP26B	*Vps26b*	3	0.7	0.0178					
8-week-old									
D3Z780	*Eif2b4*	1	> 10.0	0.0112	Q3UGB5	*Dazap1*	1	−7.4	0.0428
CDD	*Cda*	2	> 10.0	0.0102	S4R2L0	*Scgb2b12*	3	−2.6	0.0392
G3X8R0	*Reep5*	1	> 10.0	0.0122	RGL3	*Rgl3*	3	−2.1	0.0103
AP3B1	*Ap3b1*	2	> 10.0	0.0069	IDH3A	*Idh3a*	3	−1.9	0.0346
MUG1	*Mug1*	38	3.0	0.0149	RET3	*Rbp3*	1	−1.7	< 0.0001
ARL2	*Arl2*	2	2.9	0.0282	OCTC	*Crot*	16	−1.7	0.0421
TAGL	*Tagln*	2	2.9	0.0143	ACBD6	*Acbd6*	6	−1.7	0.0445
HEAT3	*Heatr3*	2	2.3	0.0343	O35176	*Scgb1b2*	8	−1.5	0.0388
DNJC7	*Dnajc7*	3	2.2	0.0091	BTF3	*Btf3*	3	−1.5	0.0064
HRG	*Hrg*	4	2.1	0.0030	OPSB	*Opn1sw*	3	−1.5	0.0038
12-week-old									
F8WHW6	*Pip5k1c*	1	5.7	0.0011	MA2B1	*Man2b1*	2	−4.6	0.0135
G3UWD8	*Rchy1*	2	4.4	0.0466	RET3	*Rbp3*	1	−3.4	< 0.0001
J3QJY4	*Scgb1b3*	5	4.3	0.0174	A0A0R4J0H3	*Rbp3*	2	−3.4	< 0.0001
GBP4	*Gbp4*	1	3.3	0.0039	A2A5K2	*Pltp*	5	−3.3	0.0006
SPA3K	*Serpina3k*	5	3.2	0.0295	CDHR1	*Cdhr1*	9	−2.8	0.0003
FETUB	*Fetub*	4	2.9	0.0138	KCD12	*Kctd12*	3	−2.7	0.0019
APOH	*Apoh*	4	2.9	0.0018	UBP47	*Usp47*	7	−2.4	0.0428
A2AP	*Serpinf2*	6	2.7	0.0059	ARRS	*Sag*	58	−2.4	< 0.0001
PLMN	*Plg*	24	2.4	0.0001	ARRC	*Arr3*	12	−2.2	0.0013
Q91Z40	*Gbp7*	1	2.4	0.0017	A2MG	*A2m*	85	−2.1	0.0005

vitreous of all models (1.5 fold in hypoxic mice; 3.9 fold at 16 weeks in rod$^{\Delta Vhl}$ mice, 1.5 fold at 12 weeks in all-cone$^{\Delta Vhl}$ mice; Tables A.1, A.2, A.3) supports a potential effect on synaptic integrity. PDLI5 is a scaffold protein that is present in the postsynaptic density and has been implicated in dendritic spine shrinkage (Herrick et al., 2010) and associated with bipolar disorder (Zain et al., 2012). Interestingly, SNP25 was detected at increased levels in cerebrospinal fluid of Alzheimer's patients and was proposed as biomarker for synapse degeneration (Brinkmalm et al., 2014).

4.1. Potential VH markers for hypoxic stress in photoreceptors

VH proteins associated with a hypoxic response in photoreceptors leading to retinal degeneration may serve as markers to detect retinal conditions that favor disease development (early markers), indicate disease progression (late markers) or reveal retinal stress in general (general markers). Such a general marker might be interferon-inducible GTPase GBP2 that was upregulated at all time points in rod$^{\Delta Vhl}$ and the last two time points in all-cone$^{\Delta Vhl}$ mice (Fig. 5). Up-regulation was also reflected on the gene expression level suggesting the involvement of HIF transcription factors in controlling *Gbp2* expression. Differential regulation of GBP2 has already been described for the ageing rat retina (Van Kirk et al., 2011), in diabetic retinopathy (Freeman et al., 2010) and in conditions that may have hypoxic components (Barben et al., 2018a; Simó et al., 2014). GBP2 is also up-regulated during neuronal apoptosis in brain (Miao et al., 2017) and may prevent mitochondrial fission through interactions with dynamin-related protein 1 (Zhang et al., 2017). Since a balance between mitochondrial fission and fusion is critical for cell survival or death (Xie et al., 2018), and inhibition of mitochondrial fission may be cytoprotective against oxidative stress (O'Mealey et al., 2017), increased GBP2 levels in the VH of rod$^{\Delta Vhl}$ and all-cone$^{\Delta Vhl}$ mice may indicate an activated defense mechanism to protect retinal integrity.

CBG (*Serpina6*) was found elevated at the early time point in both rod$^{\Delta Vhl}$ (5.1 fold) and all-cone$^{\Delta Vhl}$ (2.1 fold) mice and may thus serve as an early marker of retinal hypoxic stress. Although CBG is mainly produced in liver, its expression in the central nervous system has also been reported (Jirikowski et al., 2007; Sivukhina et al., 2013). The functional significance of the increased presence of CBG in the VH remains to be shown but may relate to the regulation of local corticosterone levels, which were suggested to have neuroprotective potential in the retina (Forkwa et al., 2014).

Other members of the serine protease inhibitor family of proteins such as A2AP (*Serpinf2; alpha-2-antiplasmin)*, A1AT (*Serpina1c; alpha-1-antitrypsin 1-3*) and IC1 (*Serping1; plasma protease C1 inhibitor*) were detected at increased levels at the intermediate time point in both rod$^{\Delta Vhl}$ and all-cone$^{\Delta Vhl}$ mice and may thus serve as late markers. Interestingly, IC1 is a regulator of the complement system and a SNP in the respective gene has been associated with AMD (Ennis et al., 2008). Several other members of the 'complement and coagulation cascades' pathway were found to be enriched in rod$^{\Delta Vhl}$ and all-cone$^{\Delta Vhl}$ mice at the early time point (Table 2) indicating a potential contribution of the complement system to retinal stress and/or degeneration in the rod$^{\Delta Vhl}$ and all-cone$^{\Delta Vhl}$ mice (see below).

4.2. Notable up-regulated proteins in the VH of rod$^{\Delta Vhl}$ mice

In addition to GBP2, increased levels of A2MG and GBP1 (Table 4,

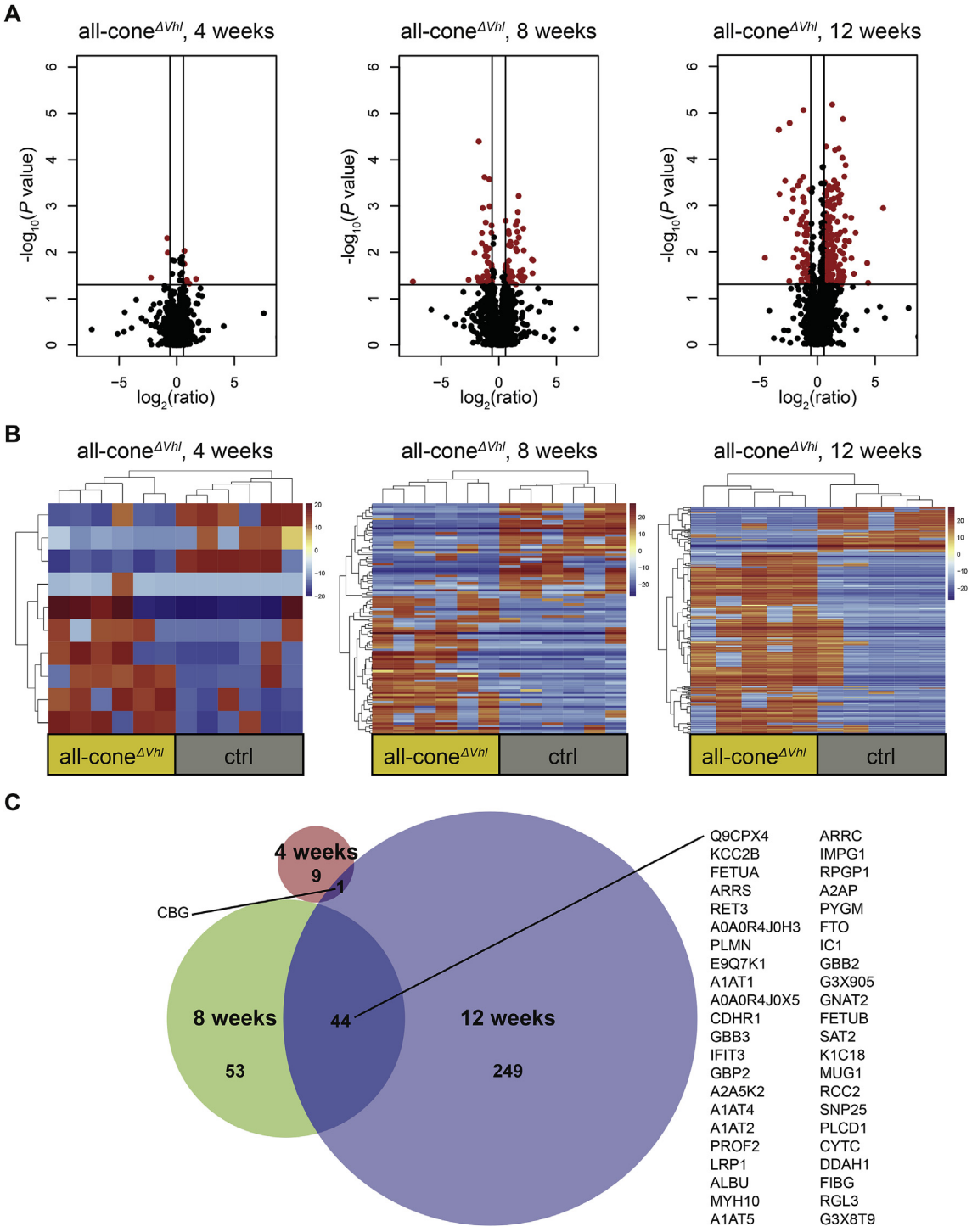

Fig. 3. Changes of the vitreous proteome in all-cone$^{\Delta Vhl}$ mice during ageing. A) Volcano plot of all identified proteins. Significantly differentially regulated proteins ($|\log_2(FC)| > 0.58$, x-axis; $P < 0.05$ ($-\log_{10}$), y-axis) are shown in red. **B)** Heat map representation with hierarchical clustering of Pearson correlation all significantly differentially regulated proteins (rows) in individual mice (columns). Shades of red: up-regulated proteins; shades of blue: down-regulated proteins by *Vhl* knockdown in cones. Columns marked with yellow represent rod$^{\Delta Vhl}$ samples, columns marked in grey represent controls. **C)** Venn diagram of significantly differentially regulated proteins ($|\log_2(FC)| > 0.58$; $P < 0.05$) of all-cone$^{\Delta Vhl}$ mice at indicated time points. N = 5–6.

A.2) were detected at all time points in rod$^{\Delta Vhl}$ mice. Since corresponding mRNA levels were also increased, rods may express and regulate A2MG and GBP1 in a HIF-dependent manner (Fig. 5B). A2MG is a ligand for low density lipoprotein receptor-related protein 1 and was assigned several functions including activation of Müller glia cells (Barcelona et al., 2011; 2013). It was shown to be expressed at higher levels in a model of oxygen-induced retinal neovascularization (Sánchez et al., 2006), was increased in the VH of retinopathy of prematurity patients (Sugioka et al., 2017) and has been proposed to be a risk factor for the development of wet AMD (The Eye Disease Case-Control Study Group 1992). GBP1, on the other hand, is critical for innate immunity (Kim et al., 2011) and belongs, like GBP2, to a family of large GTPases that are induced by interferons and inflammatory cytokines such as interleukin-1β and tumor necrosis factor α

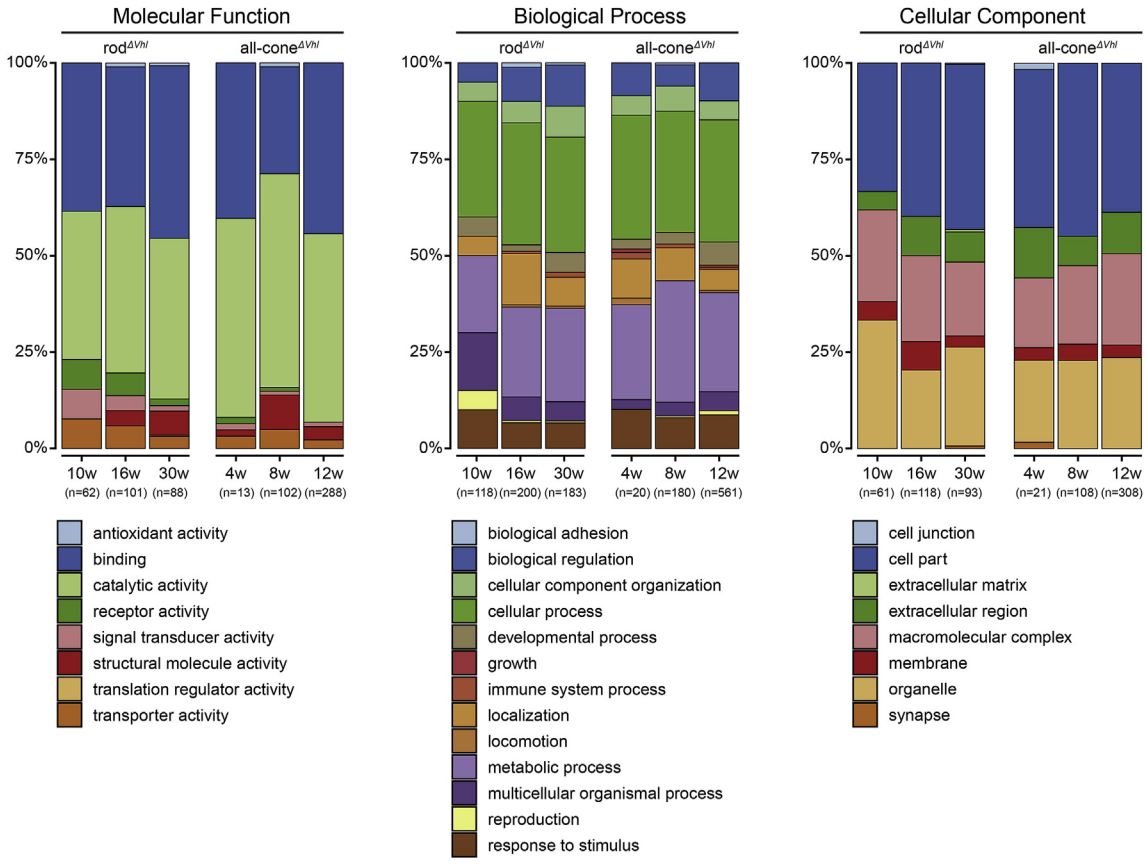

Fig. 4. GO classification of differentially regulated proteins in the VH of rod$^{\Delta Vhl}$ and all-cone$^{\Delta Vhl}$ mice. Age-dependent changes in GO-terms for 'molecular function' (GO-MF), 'biological process' (GO-BP) and 'cellular component' (GO-CC) were identified using all significantly regulated proteins in rod$^{\Delta Vhl}$ mice of 10, 16 and 30 weeks of age and in all-cone$^{\Delta Vhl}$ mice of 4, 8 and 12 weeks of age. Shown are % of total proteins (n) mapped for the particular GO-term.

(Lubeseder-Martellato et al., 2002). So far, GBP1 has not been associated with a particular eye condition.

MVP (E9Q3X9) was up-regulated strongly at the early and intermediate, but not at the late time point (Table A.2). MVP is the main component of large ribonucleoparticles known as vaults that are involved in various cellular processes such as transport, signaling and immune response (Berger et al., 2009). MVP forms a complex with HIF1A (Iwashita et al., 2010) and is involved in hypoxia-induced chemoresistance of cervical tumors (Lara et al., 2009). Thus, presence of MVP in the VH of rod$^{\Delta Vhl}$ mice may reflect the early molecular response of rods to hypoxia.

4.3. Notable up-regulated proteins in the VH of all-cone$^{\Delta Vhl}$ mice

10 differentially regulated proteins were identified in 4-week-old all-cone$^{\Delta Vhl}$ mice. Among these only calponin-3 (CNN3), a ubiquitously expressed F-actin binding protein showed a trend towards upregulation also at the later time points (Table A.3). CNN3 is suggested to be regulated by hypoxia (Appel et al., 2014), is highly expressed in brain (Ferhat et al., 1996) and has been associated with stress fiber formation and remodeling (Daimon et al., 2013). GBP2, SNP25 and SPA3N were among the proteins that were up-regulated at the intermediate and late time points (Table A.3). Their increased presence in the VH was also reflected on the gene expression level (Fig. 5). SPA3N is a serine protease inhibitor, which has neuroprotective potential by inhibiting neurotoxic granzyme B (GrB) protease activity (Haile et al., 2015). Hence, it might be produced in the retina to counteract degeneration. GBP2 and SNP25 have been addressed above.

4.4. The role of the complement cascade

As identified by gene set enrichment, activation of the 'complement and coagulation cascade' may be important early during the degeneration in rod$^{\Delta Vhl}$ and all-cone$^{\Delta Vhl}$ mice (Table 2). Three protein members of the complement system (CFAD (*Cfd*), CO4B (*C4b*) and CFAI (*Cfi*)) were commonly upregulated in both mouse strains. Others like CFAH (*Cfh*) or complement C3 (*C3*) were more specific for rod$^{\Delta Vhl}$ or all-cone$^{\Delta Vhl}$ mice, respectively. This pronounced early activation of the complement system was reflected by GO-BP analysis, in which the number of mapped proteins to 'immune system process' was highest for the early time point in rod$^{\Delta Vhl}$ mice and gradually decreased thereafter. Deregulation of the complement system has been linked to AMD (Anderson et al., 2010) and genome wide association studies have identified several single nucleotide polymorphisms in genes of the complement system to be risk factors for the development of AMD (Clark and Bishop 2017) and proliferative diabetic retinopathy (Jha et al., 2007). The identification of the complement system as regulated pathway in our models suggests that a chronic molecular response to hypoxia in photoreceptors can influence the regulation of complement factors in the eye.

4.5. Comparing the mouse to the human vitreous proteome

Orthologs of 31% of the proteins we identified earlier in human VH (Schori et al., 2018) were also identified in both genetic mouse models used here (data not shown). Of those, only four proteins remained when the comparison was limited to significantly differentially regulated proteins. Delta-aminolevulinic acid dehydratase (HEM2) was found in both rod$^{\Delta Vhl}$ mice and dry AMD, cathepsin B (CATB) and spondin-1

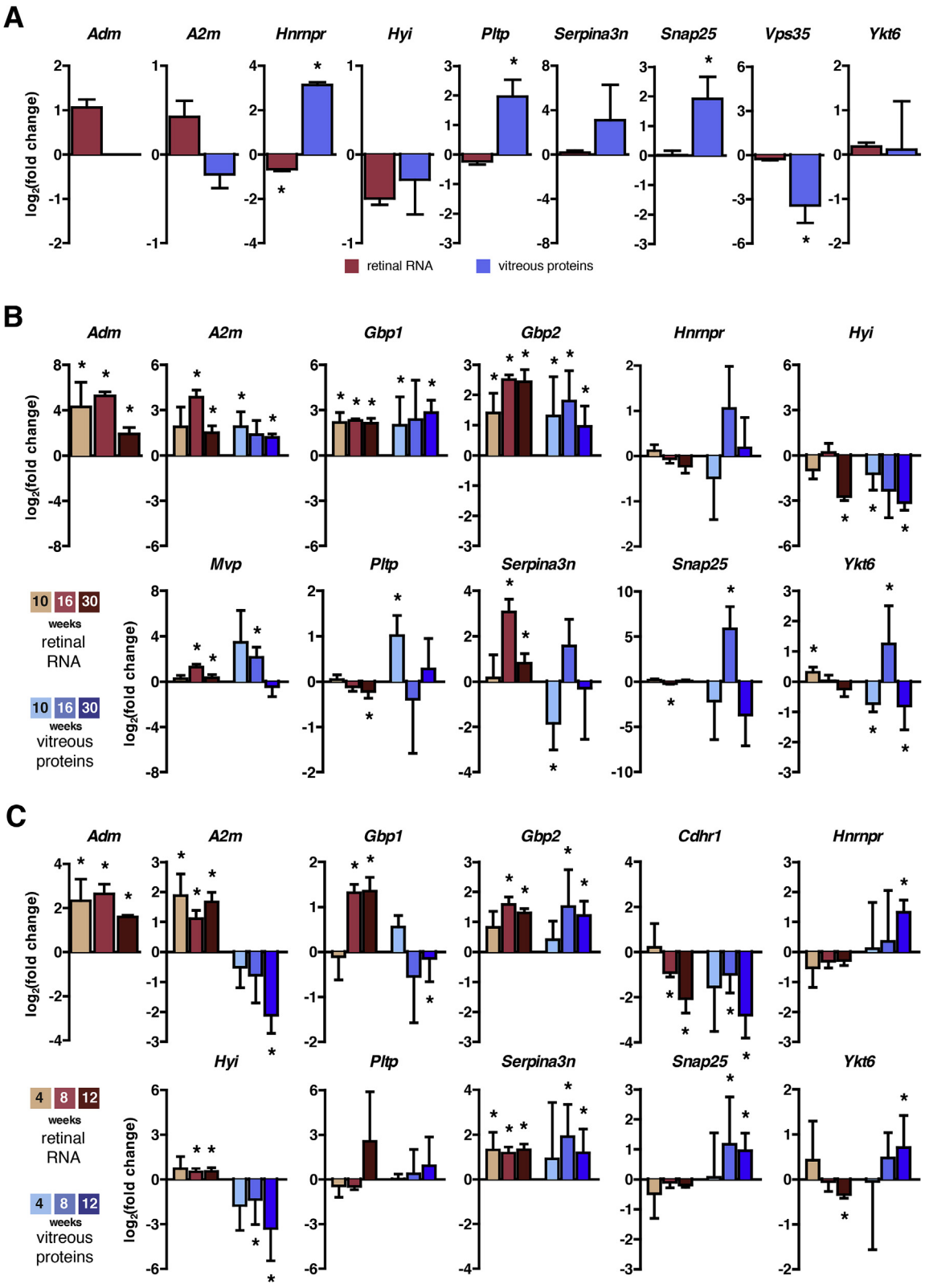

Fig. 5. Comparison of vitreous protein levels with retinal gene expression. mRNA levels (red columns) were determined in retinal samples by real-time PCR, normalized to *Actb* and expressed relative to their controls. Protein levels in the vitreous (blue columns) were determined by shot-gun proteomics and expressed relative to their controls. **A)** wild type mice exposed to acute hypoxia compared to normoxic controls (N = 3 (RNA), N = 3 (proteins)). **B)** rod$^{\Delta Vhl}$ mice at 10, 16 and 30 weeks of age (N = 3 (RNA), N = 5 (proteins)). **C)** all-cone$^{\Delta Vhl}$ mice at 4, 8 and 12 weeks of age (N = 3 (RNA), N = 6 (proteins (4 and 8 week), N = 5 (proteins 12 week)). For simplicity, gene names were used. *Adm* was amplified as a control for hypoxic gene induction in all samples analyzed. Shown are means ± SD. *: $P < 0.05$.

(SPON1) were identified in rod$^{\Delta Vhl}$ mice and wet AMD, and chitinase-3-like protein 1 (CH3L1) was common to all-cone$^{\Delta Vhl}$ mice and wet AMD (Schori et al., 2018). HEM2 is involved in catalyzing the condensation of delta-aminolevulinic acid (ALA) to porphobilinogen (Jaffe et al., 2001). This activity may reduce oxidative stress as auto-oxidation of ALA is a potential source of ROS (Princ et al., 1998). CATB is a lysosomal cysteine-protease, which plays a critical role in neuronal death through lysosomal leakage or excessive autophagy (Koike et al., 2008; Sun et al., 2010). SPON1 is involved in extracellular matrix organization (Pagnotta et al., 2013) and potentially induced by VEGF (Tratwal et al., 2015). CH3L1, the only protein found upregulated in the vitreous proteome of all-cone$^{\Delta Vhl}$ mice and wet AMD is likely reflecting the inflammation involved in disease progression of AMD (reviewed in (Kauppinen et al., 2016):). The comparison of AMD patients with mouse models of a chronically active hypoxic response in photoreceptors may be most relevant for the early time points when the retina of mice is still structurally intact. At later time points and ongoing degeneration, identified proteins may originate from degenerative processes rather than from the chronically activated hypoxic response. In addition, the strong vascular component in the pathology of all-cone$^{\Delta Vhl}$ mice (Barben et al., 2018b) adds to the complexity of the phenotype in these mice, rendering a direct comparison to the human situation difficult.

Clearly, proteins identified in this screen still need to be extensively validated before they can be considered as markers that indicate a chronic hypoxic state of photoreceptors in mice. Even more experimentation is required to test whether similar proteins are differentially present in VH of AMD patients and normal controls.

Acknowledgments

We thank Sarah Nötzli, Andrea Gubler and Coni Imsand for excellent technical assistance. This work was supported by a grant from Novartis Pharma, Switzerland, the Robert and Rosa Pulfer Foundation (Switzerland) and by the Swiss National Science Foundation (31003A_149311 and 31003A_173008). The authors declare no competing interests.

Appendix A. Supplementary data

Supplementary data to this article can be found online at https://doi.org/10.1016/j.exer.2019.107690.

References

Alm, A., Bill, A., 1972. The oxygen supply to the retina. II. Effects of high intraocular pressure and of increased arterial carbon dioxide tension on uveal and retinal blood flow in cats. A study with radioactively labelled microspheres including flow determinations in brain and. Acta Physiol. Scand. 84, 306–319.

Anderson, D.H., Radeke, M.J., Gallo, N.B., Chapin, E.A., Johnson, P.T., Curletti, C.R., Hancox, L.S., Hu, J., Ebright, J.N., Malek, G., Hauser, M.A., Rickman, C.B., Bok, D., Hageman, G.S., Johnson, L.V., 2010. The pivotal role of the complement system in aging and age-related macular degeneration: hypothesis re-visited. Prog. Retin. Eye Res. 29, 95–112.

Appel, S., Ankerne, J., Appel, J., Oberthuer, A., Mallmann, P., Dötsch, J., 2014. CNN3 regulates trophoblast invasion and is upregulated by hypoxia in BeWo cells. PLoS One 9, e103216.

Aretz, S., Krohne, T.U., Kammerer, K., Warnken, U., Hotz-Wagenblatt, A., Bergmann, M., Stanzel, B.V., Kempf, T., Holz, F.G., Schnölzer, M., Kopitz, J., 2013. In-depth mass spectrometric mapping of the human vitreous proteome. Proteome Sci. 11, 22.

Arjamaa, O., Nikinmaa, M., Salminen, A., Kaarniranta, K., 2009. Regulatory role of HIF-1alpha in the pathogenesis of age-related macular degeneration (AMD). Ageing Res. Rev. 8, 349–358.

Barben, M., Ail, D., Storti, F., Klee, K., Schori, C., Samardzija, M., Michalakis, S., Biel, M., Meneau, I., Blaser, F., Barthelmes, D., Grimm, C., 2018a. Hif1a inactivation rescues photoreceptor degeneration induced by a chronic hypoxia-like stress. Cell Death Differ 25, 2071–2085.

Barben, M., Schori, C., Samardzija, M., Grimm, C., 2018b. Targeting Hif1a rescues cone degeneration and prevents subretinal neovascularization in a model of chronic hypoxia. Mol. Neurodegener. 13, 12.

Barcelona, P.F., Jaldín-Fincati, J.R., Sánchez, M.C., Chiabrando, G.A., 2013. Activated α2-macroglobulin induces Müller glial cell migration by regulating MT1-MMP activity through LRP1. FASEB J 27, 3181–3197.

Barcelona, P.F., Ortiz, S.G., Chiabrando, G.A., Sánchez, M.C., 2011. alpha2-Macroglobulin induces glial fibrillary acidic protein expression mediated by low-density lipoprotein receptor-related protein 1 in Müller cells. Invest. Ophthalmol. Vis. Sci. 52, 778–786.

Bensaad, K., Favaro, E., Lewis, C.A., Peck, B., Lord, S., Collins, J.M., Pinnick, K.E., Wigfield, S., Buffa, F.M., Li, J.-L., Zhang, Q., Wakelam, M.J.O., Karpe, F., Schulze, A., Harris, A.L., 2014. Fatty acid uptake and lipid storage induced by HIF-1α contribute to cell growth and survival after hypoxia-reoxygenation. Cell Rep. 9, 349–365.

Berger, W., Steiner, E., Grusch, M., Elbling, L., Micksche, M., 2009. Vaults and the major vault protein: novel roles in signal pathway regulation and immunity. Cell. Mol. Life Sci. 66, 43–61.

Brinkmalm, A., Brinkmalm, G., Honer, W.G., Frölich, L., Hausner, L., Minthon, L., Hansson, O., Wallin, A., Zetterberg, H., Blennow, K., Öhrfelt, A., 2014. SNAP-25 is a promising novel cerebrospinal fluid biomarker for synapse degeneration in Alzheimer's disease. Mol. Neurodegener. 9, 53.

Brown, D.M., Kaiser, P.K., Michels, M., Soubrane, G., Heier, J.S., Kim, R.Y., Sy, J.P., Schneider, S., ANCHOR Study Group, 2006. Ranibizumab versus verteporfin for neovascular age-related macular degeneration. N. Engl. J. Med. 355, 1432–1444.

Caprara, C., Grimm, C., 2012. From oxygen to erythropoietin: relevance of hypoxia for retinal development, health and disease. Prog. Retin. Eye Res. 31, 89–119.

Cases, O., Obry, A., Ben-Yacoub, S., Augustin, S., Joseph, A., Toutirais, G., Simonutti, M., Christ, A., Cosette, P., Kozyraki, R., 2017. Impaired vitreous composition and retinal pigment epithelium function in the FoxG1::LRP2 myopic mice. Biochim. Biophys. Acta (BBA) - Mol. Basis Dis. 1863, 1242–1254.

Choksi, S., Lin, Y., Pobezinskaya, Y., Chen, L., Park, C., Morgan, M., Li, T., Jitkaew, S., Cao, X., Kim, Y.-S., Kim, H.-S., Levitt, P., Shih, G., Birre, M., Deng, C.-X., Liu, Z.-G., 2011. A HIF-1 target, ATIA, protects cells from apoptosis by modulating the mitochondrial thioredoxin, TRX2. Mol. Cell 42, 597–609.

Chung, S.E., Kang, S.W., Lee, J.H., Kim, Y.T., 2011. Choroidal thickness in polypoidal choroidal vasculopathy and exudative age-related macular degeneration. Ophthalmology 118, 840–845.

Clark, S.J., Bishop, P.N., 2017. The eye as a complement dysregulation hotspot. Semin. Immunopathol 84, 65–76.

Daimon, E., Shibukawa, Y., Wada, Y., 2013. Calponin 3 regulates stress fiber formation in dermal fibroblasts during wound healing. Arch. Dermatol. Res. 305, 571–584.

Ennis, S., Jomary, C., Mullins, R., Cree, A., Chen, X., Macleod, A., Jones, S., Collins, A., Stone, E., Lotery, A., 2008. Association between the SERPING1 gene and age-related macular degeneration: a two-stage case-control study. Lancet (London, England) 372, 1828–1834.

Feigl, B., 2009. Age-related maculopathy - linking aetiology and pathophysiological changes to the ischaemia hypothesis. Prog. Retin. Eye Res. 28, 63–86.

Ferhat, L., Charton, G., Represa, A., Ben-Ari, Y., der Terrossian, E., Khrestchatisky, M., 1996. Acidic calponin cloned from neural cells is differentially expressed during rat brain development. Eur. J. Neurosci 8, 1501–1509.

Ferris, F.L., Fine, S.L., Hyman, L., 1984. Age-related macular degeneration and blindness due to neovascular maculopathy. Arch. Ophthalmol. 102, 1640–1642.

Forkwa, T.K., Neumann, I.D., Tamm, E.R., Ohlmann, A., Reber, S.O., 2014. Short-term psychosocial stress protects photoreceptors from damage via corticosterone-mediated activation of the AKT pathway. Exp. Neurol. 252, 28–36.

Freeman, W.M., Bixler, G.V., Brucklacher, R.M., Lin, C.-M., Patel, K.M., VanGuilder, H.D., LaNoue, K.F., Kimball, S.R., Barber, A.J., Antonetti, D.A., Gardner, T.W., Bronson, S.K., 2010. A multistep validation process of biomarkers for preclinical drug development. Pharmacogenomics J. 10, 385–395.

Friedman, E., Kopald, H.H., Smith, T.R., 1964. Retinal and choroidal blood flow determined with Krypton-85 anesthetized animals. Investig. Ophthalmol. 3, 539–547.

Gao, B.-B.B., Chen, X., Timothy, N., Aiello, L.P., Feener, E.P., 2008. Characterization of the vitreous proteome in diabetes without diabetic retinopathy and diabetes with proliferative diabetic retinopathy. J. Proteome Res. 7, 2516–2525.

Greer, S.N., Metcalf, J.L., Wang, Y., Ohh, M., 2012. The updated biology of hypoxia-inducible factor. EMBO J. 31, 2448–2460.

Grimm, C., Wenzel, A., Groszer, M., Mayser, H., Seeliger, M., Samardzija, M., Bauer, C., Gassmann, M., Remé, C.E., 2002. HIF-1-induced erythropoietin in the hypoxic retina protects against light-induced retinal degeneration. Nat. Med. 8, 718–724.

Haile, Y., Carmine-Simmen, K., Olechowski, C., Kerr, B., Bleackley, R.C., Giuliani, F., 2015. Granzyme B-inhibitor serpina3n induces neuroprotection in vitro and in vivo. J. Neuroinflammation 12, 157.

Heier, J.S., Antoszyk, A.N., Pavan, P.R., Leff, S.R., Rosenfeld, P.J., Ciulla, T.A., Dreyer, R.F., Gentile, R.C., Sy, J.P., Hantsbarger, G., Shams, N., 2006. Ranibizumab for treatment of neovascular age-related macular degeneration: a phase I/II multicenter, controlled, multidose study. Ophthalmology 113 633.e1-4.

Herrick, S., Evers, D.M., Lee, J.-Y., Udagawa, N., Pak, D.T.S., 2010. Postsynaptic PDLIM5/Enigma Homolog binds SPAR and causes dendritic spine shrinkage. Mol. Cell. Neurosci. 43, 188–200.

Hirano, A.A., Brandstätter, J.H., Morgans, C.W., Brecha, N.C., 2011. SNAP25 expression in mammalian retinal horizontal cells. J. Comp. Neurol. 519, 972–988.

Hu, Q., Liang, X., Chen, D., Chen, Y., Doycheva, D., Tang, J., Tang, J., Zhang, J.H., 2014. Delayed hyperbaric oxygen therapy promotes neurogenesis through reactive oxygen species/hypoxia-inducible factor-1α/β-catenin pathway in middle cerebral artery occlusion rats. Stroke 45, 1807–1814.

Hulsen, T., de Vlieg, J., Alkema, W., 2008. BioVenn - a web application for the comparison and visualization of biological lists using area-proportional Venn diagrams. BMC Genomics 9, 488.

Hwang, I.I.L., Watson, I.R., Der, S.D., Ohh, M., 2006. Loss of VHL confers hypoxia-inducible factor (HIF)-dependent resistance to vesicular stomatitis virus: role of HIF in antiviral response. J. Virol. 80, 10712–10723.

Iwashita, K. ichi, Ikeda, R., Takeda, Y., Sumizawa, T., Furukawa, T., Yamaguchi, T.,

Akiyama, S. ichi, Yamada, K., 2010. Major vault protein forms complexes with hypoxia-inducible factor (HIF)-1α and reduces HIF-1α level in ACHN human renal adenocarcinoma cells. Cancer Sci. 101, 920–926.
Jaffe, E.K., Martins, J., Li, J., Kervinen, J., Dunbrack, R.L., 2001. The molecular mechanism of lead inhibition of human porphobilinogen synthase. J. Biol. Chem. 276, 1531–1537.
Jha, P., Bora, P.S., Bora, N.S., 2007. The role of complement system in ocular diseases including uveitis and macular degeneration. Mol. Immunol 44, 3901–3908.
Jirikowski, G.F., Pusch, L., Möpert, B., Herbert, Z., Caldwell, J.D., 2007. Expression of corticosteroid binding globulin in the rat central nervous system. J. Chem. Neuroanat. 34, 22–28.
Käll, L., Storey, J.D., MacCoss, M.J., Noble, W.S., 2008. Assigning significance to peptides identified by tandem mass spectrometry using decoy databases. J. Proteome Res. 7, 29–34.
Kauppinen, A., Paterno, J.J., Blasiak, J., Salminen, A., Kaarniranta, K., 2016. Inflammation and its role in age-related macular degeneration. Cell. Mol. Life Sci. 73, 1765–1786.
Kim, B.-H., Shenoy, A.R., Kumar, P., Das, R., Tiwari, S., MacMicking, J.D., 2011. A family of IFN-γ-inducible 65-kD GTPases protects against bacterial infection. Science 332, 717–721.
Koike, M., Shibata, M., Tadakoshi, M., Gotoh, K., Komatsu, M., Waguri, S., Kawahara, N., Kuida, K., Nagata, S., Kominami, E., Tanaka, K., Uchiyama, Y., 2008. Inhibition of autophagy prevents hippocampal pyramidal neuron death after hypoxic-ischemic injury. Am. J. Pathol. 172, 454–469.
Koss, M.J., Hoffmann, J., Nguyen, N., Pfister, M., Mischak, H., Mullen, W., Husi, H., Rejdak, R., Koch, F., Jankowski, J., Krueger, K., Bertelmann, T., Klein, J., Schanstra, J.P., Siwy, J., 2014. Proteomics of vitreous humor of patients with exudative age-related macular degeneration. PLoS One 9, e96895.
Kurihara, T., Westenskow, P.D., Gantner, M.L., Usui, Y., Schultz, A., Bravo, S., Aguilar, E., Wittgrove, C., Friedlander, M.S.H., Paris, L.P., Chew, E., Siuzdak, G., Friedlander, M., 2016. Hypoxia-induced metabolic stress in retinal pigment epithelial cells is sufficient to induce photoreceptor degeneration. Elife 5, 1–22.
Kutmon, M., Riutta, A., Nunes, N., Hanspers, K., Willighagen, E.L., Bohler, A., Mélius, J., Waagmeester, A., Sinha, S.R., Miller, R., Coort, S.L., Cirillo, E., Smeets, B., Evelo, C.T., Pico, A.R., 2016. WikiPathways: capturing the full diversity of pathway knowledge. Nucleic Acids Res. 44, D488–D494.
Lange, C., Heynen, S.R., Tanimoto, N., Thiersch, M., Le, Y.-Z., Meneau, I., Seeliger, M.W., Samardzija, M., Caprara, C., Grimm, C., 2011. Normoxic activation of hypoxia-inducible factors in photoreceptors provides transient protection against light-induced retinal degeneration. Invest. Ophthalmol. Vis. Sci. 52, 5872–5880.
Lara, P.C., Lloret, M., Clavo, B., Apolinario, R.M., Henríquez-Hernández, L.A., Bordón, E., Fontes, F., Rey, A., 2009. Severe hypoxia induces chemo-resistance in clinical cervical tumors through MVP over-expression. Radiat. Oncol. 4, 29.
Leibowitz, H.M., Krueger, D.E., Maunder, L.R., Milton, R.C., Kini, M.M., Kahn, H.A., Nickerson, R.J., Pool, J., Colton, T.L., Ganley, J.P., Loewenstein, J.I., Dawber, T.R., 1980. The Framingham Eye Study monograph: an ophthalmological and epidemiological study of cataract, glaucoma, diabetic retinopathy, macular degeneration, and visual acuity in a general population of 2631 adults, 1973-1975. Surv. Ophthalmol. 24, 335–610.
Linsenmeier, R.A., Padnick-Silver, L., 2000. Metabolic dependence of photoreceptors on the choroid in the normal and detached retina. Invest. Ophthalmol. Vis. Sci. 41, 3117–3123.
Liu, K., Xie, B., 2012. Today and future of age-related macular degeneration. ISRN Ophthalmol 2012, 1–9.
Loukovaara, S., Nurkkala, H., Tamene, F., Gucciardo, E., Liu, X., Repo, P., Lehti, K., Varjosalo, M., 2015. Quantitative proteomics analysis of vitreous humor from diabetic retinopathy patients. J. Proteome Res. 14, 5131–5143.
Lubeseder-Martellato, C., Guenzi, E., Jörg, A., Töpolt, K., Naschberger, E., Kremmer, E., Zietz, C., Tschachler, E., Hutzler, P., Schwemmle, M., Matzen, K., Grimm, T., Ensoli, B., Stürzl, M., 2002. Guanylate-binding protein-1 expression is selectively induced by inflammatory cytokines and is an activation marker of endothelial cells during inflammatory diseases. Am. J. Pathol 161, 1749–1759.
Ma, T., Schreiber, C.A., Knutson, G.J., Khattouti, A. El, Sakiyama, M.J., Hassan, M., Charlesworth, M.C., Madden, B.J., Zhou, X., Vuk-Pavlović, S., Gomez, C.R., 2015. Effects of oxygen on the antigenic landscape of prostate cancer cells. BMC Res. Notes 8, 687.
Man, J., Yu, X., Huang, H., Zhou, W., Xiang, C., Huang, H., Miele, L., Liu, Z., Bebek, G., Bao, S., Yu, J.S., 2018. Hypoxic induction of vasorin regulates Notch1 turnover to maintain glioma stem-like cells. Cell Stem Cell 22, 104–118 e6.
Márkus, B., Pató, Z., Sarang, Z., Albert, R., Tőzsér, J., Petrovski, G., Csősz, É., 2017. The proteomic profile of a mouse model of proliferative vitreoretinopathy. FEBS Open Bio 7, 1166–1177.
Mi, H., Huang, X., Muruganujan, A., Tang, H., Mills, C., Kang, D., Thomas, P.D., 2017. PANTHER version 11: expanded annotation data from Gene Ontology and Reactome pathways, and data analysis tool enhancements. Nucleic Acids Res. 45, D183–D189.
Miao, Q., Ge, M., Huang, L., 2017. Up-regulation of GBP2 is associated with neuronal apoptosis in rat brain cortex following traumatic brain injury. Neurochem. Res. 42, 1515–1523.
Monteiro, J.P., Santos, F.M., Rocha, A.S., Castro-de-Sousa, J.P., Queiroz, J.A., Passarinha, L.A., Tomaz, C.T., 2015. Vitreous humor in the pathologic scope: insights from proteomic approaches. Proteonomics Clin. Appl. 9, 187–202.
Nobl, M., Reich, M., Dacheva, I., Siwy, J., Mullen, W., Schanstra, J.P., Choi, C.Y., Kopitz, J.J., Kretz, F.T.A.A., Auffarth, G.U., Koch, F., Koss, M.J., 2016. Proteomics of vitreous in neovascular age-related macular degeneration. Exp. Eye Res. 146, 107–117.
O'Mealey, G.B., Berry, W.L., Plafker, S.M., 2017. Sulforaphane is a Nrf2-independent inhibitor of mitochondrial fission. Redox Biol 11, 103–110.
Pagnotta, S.M., Laudanna, C., Pancione, M., Sabatino, L., Votino, C., Remo, A., Cerulo, L., Zoppoli, P., Manfrin, E., Colantuoni, V., Ceccarelli, M., 2013. Ensemble of gene signatures identifies novel biomarkers in colorectal cancer activated through PPARγ and TNFα signaling. PLoS One 8, e72638.
Princ, F.G., Maxit, A.G., Cardalda, C., Batlle, A., Juknat, A.A., 1998. In vivo protection by melatonin against delta-aminolevulinic acid-induced oxidative damage and its antioxidant effect on the activity of haem enzymes. J. Pineal Res. 24, 1–8.
Qiang, L., Wu, T., Zhang, H.-W., Lu, N., Hu, R., Wang, Y.-J., Zhao, L., Chen, F.-H., Wang, X.-T., You, Q.-D., Guo, Q.-L., 2012. HIF-1α is critical for hypoxia-mediated maintenance of glioblastoma stem cells by activating Notch signaling pathway. Cell Death Differ. 19, 284–294.
Rosenfeld, P.J., Brown, D.M., Heier, J.S., Boyer, D.S., Kaiser, P.K., Chung, C.Y., Kim, R.Y., MARINA Study Group, 2006. Ranibizumab for neovascular age-related macular degeneration. N. Engl. J. Med. 355, 1419–1431.
Samardzija, M., Caprara, C., Heynen, S.R., Willcox DeParis, S., Meneau, I., Traber, G., Agca, C., von Lintig, J., Grimm, C., 2014. A mouse model for studying cone photoreceptor pathologies. Invest. Ophthalmol. Vis. Sci. 55, 5304–5313.
Sánchez, M.C., Barcelona, P.F., Luna, J.D., Ortiz, S.G., Juarez, P.C., Riera, C.M., Chiabrando, G.A., 2006. Low-density lipoprotein receptor-related protein-1 (LRP-1) expression in a rat model of oxygen-induced retinal neovascularization. Exp. Eye Res. 83, 1378–1385.
Schori, C., Trachsel, C., Grossmann, J., Zygoula, I., Barthelmes, D., Grimm, C., 2018. The proteomic landscape in the vitreous of patients with age-related and diabetic retinal disease. Invest. Ophthalmol. Vis. Sci. 59, AMD31–AMD40.
Sena, J. a, Wang, L., Pawlus, M.R., Hu, C.-J., 2014. HIFs enhance the transcriptional activation and splicing of adrenomedullin. Mol. Cancer Res. 12, 728–741.
Shih, S.C., Claffey, K.P., 1999. Regulation of human vascular endothelial growth factor mRNA stability in hypoxia by heterogeneous nuclear ribonucleoprotein L. J. Biol. Chem. 274, 1359–1365.
Shitama, T., Hayashi, H., Noge, S., Uchio, E., Oshima, K., Haniu, H., Takemori, N., Komori, N., Matsumoto, H., 2008. Proteome profiling of vitreoretinal diseases by cluster Analysis. Proteomics. Clin. Appl. 2, 1265–1280.
Simó, R., Sundstrom, J.M., Antonetti, D.A., 2014. Ocular Anti-VEGF therapy for diabetic retinopathy: the role of VEGF in the pathogenesis of diabetic retinopathy. Diabetes Care 37, 893–899.
Sivukhina, E., Helbling, J.-C., Minni, A.M., Schäfer, H.H., Pallet, V., Jirikowski, G.F., Moisan, M.-P., 2013. Intrinsic expression of transcortin in neural cells of the mouse brain: a histochemical and molecular study. J. Exp. Biol. 216, 245–252.
Skeie, J. m., Mahajan, V.B., 2013. Proteomic interactions in the mouse vitreous-retina complex. PLoS One 8, e82140.
Skeie, J.M., Tsang, S.H., Mahajan, V.B., 2011. Evisceration of mouse vitreous and retina for proteomic analyses. J. Vis. Exp. 12–14.
Som, A., Harder, C., Greber, B., Siatkowski, M., Paudel, Y., Fuellen, G., 2010. The PluriNetWork : an Electronic Representation of the Network Underlying Pluripotency in Mouse , and its Applications 5.
Stefánsson, E., Geirsdóttir, A., Sigurdsson, H., 2011. Metabolic physiology in age related macular degeneration. Prog. Retin. Eye Res. 30, 72–80.
Subramanian, A., Tamayo, P., Mootha, V.K., Mukherjee, S., Ebert, B.L., Gillette, M.A., Paulovich, A., Pomeroy, S.L., Golub, T.R., Lander, E.S., Mesirov, J.P., 2005. Gene set enrichment analysis: a knowledge-based approach for interpreting genome-wide expression profiles. Proc. Natl. Acad. Sci. Unit. States Am. 102, 15545–15550.
Sugioka, K., Saito, A., Kusaka, S., Kuniyoshi, K., Shimomura, Y., 2017. Identification of vitreous proteins in retinopathy of prematurity. Biochem. Biophys. Res. Commun 488, 483–488.
Sun, L., Wu, Z., Baba, M., Peters, C., Uchiyama, Y., Nakanishi, H., 2010. Cathepsin B-dependent motor neuron death after nerve injury in the adult mouse. Biochem. Biophys. Res. Commun. 399, 391–395.
Tratwal, J., Mathiasen, A.B., Juhl, M., Brorsen, S.K., Kastrup, J., Ekblond, A., 2015. Influence of vascular endothelial growth factor stimulation and serum deprivation on gene activation patterns of human adipose tissue-derived stromal cells. Stem Cell Res. Ther. 6, 62.
Türker, C., Akal, F., Joho, D., Panse, C., Barkow-Oesterreicher, S., Rehrauer, H., Schlapbach, R., 2010. B-Fabric. In: Proceedings of the 13th International Conference on Extending Database Technology - EDBT '10. ACM Press, New York, New York, USA, pp. 717.
Van Kirk, C.A., VanGuilder, H.D., Young, M., Farley, J.A., Sonntag, W.E., Freeman, W.M., 2011. Age-related alterations in retinal neurovascular and inflammatory transcripts. Mol. Vis. 17, 1261–1274.
Vizcaíno, J.A., Csordas, A., Del-Toro, N., Dianes, J.A., Griss, J., Lavidas, I., Mayer, G., Perez-Riverol, Y., Reisinger, F., Ternent, T., Xu, Q.-W., Wang, R., Hermjakob, H., 2016. 2016 update of the PRIDE database and its related tools. Nucleic Acids Res. 44, D447–D456.
Wang, H., Feng, L., Hu, J., Xie, C., Wang, F., 2013. Differentiating vitreous proteomes in proliferative diabetic retinopathy using high-performance liquid chromatography coupled to tandem mass spectrometry. Exp. Eye Res. 108, 110–119.
Wang, J., Vasaikar, S., Shi, Z., Greer, M., Zhang, B., 2017. WebGestalt 2017: a more comprehensive, powerful, flexible and interactive gene set enrichment analysis toolkit. Nucleic Acids Res. 45, W130–W137.
Wiśniewski, J.R., Zougman, A., Nagaraj, N., Mann, M., 2009. Universal sample preparation method for proteome analysis. Nat. Methods 6, 359–362.
Wong, W.L., Su, X., Li, X., Cheung, C.M.G., Klein, R., Cheng, C.-Y.Y., Wong, T.Y., 2014. Global prevalence of age-related macular degeneration and disease burden projection for 2020 and 2040: a systematic review and meta-analysis. Lancet. Glob. Heal. 2, e106–e116.
Xie, L.-L., Shi, F., Tan, Z., Li, Y., Bode, A.M., Cao, Y., 2018. Mitochondrial network structure homeostasis and cell death. Cancer Sci. 109, 3686–3694.

Yamane, K., Minamoto, A., Yamashita, H., Takamura, H., Miyamoto-Myoken, Y., Yoshizato, K., Nabetani, T., Tsugita, A., Mishima, H.K., 2003. Proteome analysis of human vitreous proteins. Mol. Cell. Proteom. 2, 1177–1187.
Zain, M.A., Jahan, S.N., Reynolds, G.P., Zainal, N.Z., Kanagasundram, S., Mohamed, Z., 2012. Peripheral PDLIM5 expression in bipolar disorder and the effect of olanzapine administration. BMC Med. Genet. 13, 91.
Zhang, J., Zhang, Y., Wu, W., Wang, F., Liu, X., Shui, G., Nie, C., 2017. Guanylate-binding protein 2 regulates Drp1-mediated mitochondrial fission to suppress breast cancer cell invasion. Cell Death Dis. 8, e3151.